For submission to *Marine Ecology Progress Series* December 10, 2010:

CLIMATE CONTROLS ON THE GIANT KELP POPULATIONS OF THE SANTA BARBARA CHANNEL, CALIFORNIA

KYLE C. CAVANAUGH [1,*], DAVID A. SIEGEL[1,2], DANIEL C. REED[3], PHILIP E. DENNISON[4]

[1]*Earth Research Institute, University of California, Santa Barbara, California, USA 93106*

[2]*Department of Geography, University of California, Santa Barbara, California, USA 93106*

[3]*Marine Science Institute, University of California, Santa Barbara, California, USA 93106*

[4]*Department of Geography, University of Utah, USA 84112*

[*] Email: kyle@eri.ucsb.edu

Running Title: Climate controls on kelp populations

Keywords: Giant kelp, Spatial and temporal variability, Disturbance, Remote sensing, Long-term data

ABSTRACT

Synthesizing long-term observations at multiple spatial and temporal scales is vital to understanding and predicting ecosystem responses to a changing climate. Here, we

developed a novel method for measuring giant kelp (*Macrocystis pyrifera*) canopy biomass using LANDSAT 5 Thematic Mapper satellite imagery for the Santa Barbara Channel. The regional, 25-year mean giant kelp canopy biomass was estimated at 43700 metric tons and was highly variable (C.V. = 87%), illustrating the important role of disturbance in regulating regional scale giant kelp biomass. The canopy biomass determinations were compared with oceanographic and climatic data to assess the roles of environmental processes in determining regional and subregional giant kelp biomass. Seasonal losses and recoveries of regional kelp canopy biomass were correlated with surface gravity wave heights and sea surface temperature (r^2 = 0.50 and 0.30 respectively), the later of which is inversely related to nutrient availability. On interannual timescales, regional kelp canopy biomass lagged wave heights, sea surface temperature, and the North Pacific Gyre Oscillation (NPGO) index by 3 years, indicating potential relationships between these variables and population-level recruitment and mortality cycles. Cluster analysis demonstrated that subregions with similar temporal dynamics were largely determined by environmental conditions. The dynamics of kelp biomass in exposed subregions were related to surface wave disturbance while kelp dynamics in sheltered regions tracked sea surface temperatures more closely. This work demonstrates how long-term, high-frequency remote observations of dynamic systems such as kelp forests can be combined with physical data to better understand how physical drivers impact ecological systems in space and time.

41 # INTRODUCTION

42 Climate-related changes in the oceans appear to be accelerating: oceans are
43 becoming warmer and more acidic, nutrient distributions are changing, and, in some
44 regions such as the Northwest Pacific, the frequency and intensity of large storms are
45 increasing (e.g., Easterling et al. 2000, Behrenfeld et al. 2006, IPCC 2007a, Meehl et al.
46 2007; Doney et al. 2009). Many marine ecosystems have displayed dramatic responses
47 to recent fluctuations in climate, and accumulating evidence suggests that coastal marine
48 ecosystems are especially vulnerable to the effects of climate change (e.g., Harley et al.
49 2006, Przeslawski et al 2008; Hoegh-Guldberg and Bruno 2010). However, our
50 understanding of how climate changes will affect coastal marine ecosystems is limited.
51 Data collection in many coastal ecosystems is labor intensive and there are relatively few
52 long-term (>20 yr) studies of change in coastal marine ecosystems as compared to
53 terrestrial systems (Rosenzweig et al 2008). Increasing the number of long-term, large-
54 scale data sets on coastal ecosystems and their responses to climate changes is of critical
55 importance.

56 Among coastal primary producers, forests of giant kelp *(Macrocystis pyrifera)* are
57 particularly sensitive to climate change (Graham et al. 2007). Giant kelp is the world's
58 largest alga and its numerous fronds extend vertically in the water column and form a
59 canopy at the sea surface. Giant kelp's biomass is exceptionally dynamic; short lifespans
60 of both fronds and entire plants (4 - 6 months and 2 - 3 years, respectively) combine with
61 rapid growth (~ 2% d^{-1}) to produce a standing biomass that turns over 6 to 7 times per
62 year (Reed et al. 2008). Because of such rapid turnover, the biomass dynamics of giant
63 kelp responds quickly to changes in environmental conditions.

64 Giant kelp recruitment and growth are controlled by abotic factors including
65 substrate availability, solar radiation, water temperature, and nutrient availability as well
66 as the biotic effects of inter- and intra-species competition for space and light and grazing
67 (reviewed in Graham et al. 2007). In southern California, growth is fastest in winter and
68 spring when nutrients are high, temperature is low and competition for light and space is
69 low (due to low algal biomass) and slowest during summer when nutrients are low,
70 temperatures are high and competition for light and space is high due to well developed
71 algal canopies (Zimmerman and Kremer 1986, Reed et al. 2008). The relatively low
72 capacity of giant kelp to store nutrients (~30 days, Zimmerman and Kremer 1986) causes
73 populations to respond rapidly to fluctuations in nutrient supply. Much like growth, the
74 recruitment of giant kelp in southern California and elsewhere responds greatly to
75 fluctuations in nutrients, temperature, and light as determined by biotic and abiotic
76 processes (Dayton et al. 1984, Reed and Foster 1984, Reed et al. 2008). Giant kelp
77 produces spores throughout the year (Reed et al. 1996) and the recruitment of new plants
78 typically occurs whenever favorable conditions of light, temperature and nutrients
79 coincide (Deysher and Dean 1986).

80 Giant kelp mortality occurs in the form of senescence, trophic interactions (i.e.,
81 grazing), and surface wave-driven disturbance (Graham et al. 2007). Reed et al. (2008)
82 found that both frond losses and plant mortality were correlated to wave heights in kelp
83 forests near Santa Barbara, California. While correlated to waves, frond losses occurred
84 continuously throughout the year and significant losses occurred from senescence
85 unrelated to wave dislodgement. On the other hand, plant-level loss was episodic and
86 occurred primarily during periods of high waves. Large-scale mortality can also result

87 from extreme nutrient limitation; for example, kelp populations across southern and Baja
88 California were devastated by the warm, nutrient poor conditions of the 1983 and 1997 El
89 Niño events (Dayton & Tegner 1984, Dayton & Tegner 1989, Dayton 1999, Edwards
90 2004). The regional dynamics of giant kelp reflect the interplay of these physical and
91 biological forcings that control the mechanisms of recruitment, growth, and mortality.

92 The relative importance of resource availability (light/nutrients) vs. physical
93 disturbance (waves) in controlling the biomass dynamics of giant kelp remains an open
94 question. For example, Dayton et al. (1999) found that large-scale, low frequency
95 changes in nutrient availability had the largest effects on kelp populations in San Diego;
96 however, recent analyses of kelp forests in central and southern California during 2001-
97 2009 (a period lacking any major nutrient poor El Niño conditions) showed that wave
98 driven disturbance explained more variability in kelp biomass and production than either
99 nutrient availability or consumer pressure (Reed et al. 2008, Reed et al. in prep). It is
100 clear that the influence that each of these physical forcings has on kelp populations is
101 dependent on the spatial and temporal scales of observation (Edwards et al. 2004). The
102 vast majority of long-term kelp studies have been made at the local scale and so it has
103 been difficult to test how their conclusions apply to larger areas. In the past, aerial and
104 satellite imagery has been used to examine kelp forests at regional scales; however, these
105 studies have all been either short-term pilot studies (e.g. Deysher 1993, Stekoll et al.
106 2006) or limited to just a few years (e.g. Donnellan 2004, Cavanaugh et al. 2010), too
107 short a period to examine interannual to decadal variability in kelp biomass dynamics.

108 Here, we describe the development of a new kelp canopy biomass dataset
109 possessing unprecedented spatial and temporal resolution and extent using multispectral

imagery from the LANDSAT 5 Thematic Mapper (TM) sensor. These observations enabled the assessment of giant kelp canopy biomass at 30 m resolution across the entire Santa Barbara Channel every 1 to 2 months for 25 years (1984 to 2009). We compare these novel observations of giant kelp forests with oceanographic and climate observations to assess resource and disturbance driven controls on kelp populations at multiple spatial and temporal scales. Our objectives were to determine (1) the relative importance of resource availability and wave disturbance in driving both seasonal and interannual cycles of regional kelp biomass in the Santa Barbara Channel and (2) the level of spatial variability in the importance of these forcing processes within the Channel. We show that kelp biomass was significantly related to significant wave heights, sea surface temperatures (SST), and climate indices at seasonal to interannual timescales. We also demonstrate that these responses were spatially partitioned into distinct subregions within the Santa Barbara Channel. A picture of a complex system emerges where large-scale climate changes drive variability in temperature, nutrient levels, and surface gravity wave energy, which in turn drives spatially variable seasonal and interannual cycles in giant kelp canopy biomass. Variability in kelp biomass has been shown to impact many other trophic levels (Graham 2004, Byrnes et al. in review), thus the ecological implications of these results are far-reaching. A more complete understanding of how giant kelp forests vary in space and time will provide insight into how they affect the vast number of ecologically and economically important species associated with them.

METHODS

133 **Study site**

134 We used available LANDSAT 5 TM satellite imagery to track giant kelp canopy
135 biomass across the entire Santa Barbara Channel from 1984 to 2009. The study area
136 included the coastline from Pismo Beach, CA to Oxnard, CA and each of the northern
137 Channel Islands (Figure 1). Oceanographic conditions over this region are highly
138 dynamic in space and time (Harms and Winant, 1998, Otero and Siegel, 2004); thus the
139 region represents an ideal system in which to investigate the importance of physical
140 controls on the spatiotemporal distributions of giant kelp populations.

141 The Santa Barbara Channel experiences pronounced seasonal cycles in sea
142 surface temperature, nutrient conditions, and wave energy. During the winter, major
143 storms move across the Northwest Pacific and send large northwesterly swells into the
144 Santa Barbara Channel. Wave energy from these storms is a major source of giant kelp
145 mortality in the region (Reed et al. 2008). Nutrient levels are relatively high in the winter
146 as a deepening of the mixed layer entrains nutrients into surface waters. Spring
147 represents a period of transition in the wave climate of the Santa Barbara Channel as the
148 frequency of large northwesterly wave events decreases, giving way to smaller southerly
149 swells that are characteristic of summer months (Adams et al. 2008). Nutrient levels in
150 the nearshore regions generally reach maximums during spring months due to coastal
151 upwelling. The role of upwelling in providing nutrients and rapid incorporation by
152 biological processes leads to a strong negative relationship between SST and nutrient
153 levels (McPhee-Shaw et al. 2007). During the summer and fall, vertical stratification
154 increases creating warmer temperatures and lower nutrient levels (e.g., McPhee-Shaw et

155 al. 2007, Fram et al. 2008). Less intense southerly swells are common in the summer
156 months and can affect exposed south-facing coastlines.

157 The seasonal cycles in resource availability and physical disturbance are super-
158 imposed on longer period cycles driven by El Niño/Southern Oscillation (SOI), Pacific
159 Decadal Oscillation (PDO), and North Pacific Gyre Oscillation (NPGO) events. These
160 climate cycles alter seawater temperatures, nutrient levels, and storm patterns, and can
161 have dramatic effects on kelp populations (e.g., Dayton & Tegner 1990, Edwards 2004).
162 El Niños generally correspond with a deepening of mixed layer, reduced upwelling,
163 warmer surface waters, and reduced ecosystem productivity along the U.S. west coast
164 (Barber and Chavez 1983). Strong El Niño years have also been shown to produce
165 stronger winter storms that take more southerly tracks across the North Pacific, resulting
166 in larger wave events along the coast of Southern California (Seymour 1998, Adams
167 2008). The PDO is a longer period cycle that changes state every 20-40 years (Mantua
168 and Hare 2002); positive phases generally correspond with increased SST. Whereas the
169 PDO represents the 1st mode of sea surface height variability in the Northeast Pacific and
170 is the dominant signal in physical parameters such as SST, the recently identified NPGO
171 is the 2nd mode of sea surface height variability and is better correlated with ecosystem
172 productivity metrics such as nutrient levels, salinity, and phytoplankton chlorophyll (Di
173 Lorenzo et al. 2008, 2009). All of the above climate cycles control large-scale, low
174 frequency changes in physical variables important to kelp populations.

175 The Santa Barbara Channel also experiences a great deal of spatial variability in
176 oceanographic conditions. The region is located at the convergence of the equatorward
177 flowing California Current and the recirculating Southern California Eddy and Inshore

178 Countercurrent (Hickey 1979). Strong upwelling north of Pt. Conception creates cool,
179 nutrient rich conditions throughout most of the year while regions in the eastern portion
180 of the Channel experience warmer, more nutrient limited conditions during summer
181 months (Otero and Siegel, 2004). While there is spatial variability in the SST of the Santa
182 Barbara Channel, the vast majority of the region's temporal variability is homogeneous
183 across the entire channel (Otero and Siegel 2004, see below).

184 Even more dramatic is the spatial variability in wave exposure. Again, Point
185 Conception represents a natural boundary: the coastline north of Pt. Conception is
186 exposed to both powerful winter northwest swells as well as weaker summer southern
187 swells while the coastline south of Pt. Conception is sheltered from northern swells by Pt.
188 Conception and from southern swells by the Channel Islands (O'Reilly and Guza 1993).
189 The Channel Islands themselves present a myriad of exposures, but in general the north
190 sides of the islands are exposed to northwest swells and sheltered from southern swells,
191 while the opposite is true for the south facing sides of the islands. It is important to note
192 that while the above descriptions depict wave exposure in general, the precise spatial
193 distribution of wave energy along the coast of our study area depends on the specific
194 direction of a given swell (Adams et al. 2008). As with SST and nutrients, large, long-
195 period swells affect the entire Channel, but to varying degrees due to the large amount of
196 spatial variability in wave exposure. Clearly, subtidal ecosystems of the Santa Barbara
197 Channel such as giant kelp experience physical conditions that vary substantially in space
198 and time.

199

200 **Satellite estimation of giant kelp canopy biomass**

201 Giant kelp forms a dense floating surface canopy that is distinctive when viewed
202 from above. In our study area, giant kelp is the only canopy forming macrophyte in
203 water depths from 5 to 30 m. This greatly simplifies its quantification from satellite
204 imagery. The spectral signature of a giant kelp canopy is similar to that of
205 photosynthetically active terrestrial vegetation, namely a high near infrared and
206 significantly lower visible reflectance (Jensen et al. 1980; Cavanaugh et al. 2010). Water
207 absorbs almost all incoming near-infrared energy so kelp canopy is easily differentiated
208 using its near-infrared reflectance signal.

209 The LANDSAT 5 TM sensor has acquired 30 m spatial resolution multispectral
210 imagery nearly continuously from 1984 to the present on a 16-day repeat cycle
211 (Markham et al. 2004). TM obtains data in 7 spectral bands: blue (450-520 nm), green
212 (520-600 nm), red (630-690 nm), near infrared (760-900), shortwave infrared (1500-1750
213 and 2080-2350 nm), and longwave (thermal) infrared (10400-12500 nm)
214 (http://landsat.gsfc.nasa.gov/about/tm.html). TM data is stored as 8-bit encoded radiance,
215 with 256 possible "brightness values" representing the range of radiance for each band.
216 The kelp near infrared (band 4) radiance signal, while strong compared to that of water,
217 spans only the lowest ~40 brightness values detectable by TM. Each LANDSAT scene
218 covers an area 170 x 180 km; the scene we used for this study included the entire study
219 area described above (Figure 1). During preprocessing, LANDSAT images were
220 geometrically corrected using ground control points and a digital elevation model to
221 achieve a scene-to-scene registration accuracy < 7.3 m (Lee et al. 2004). We selected
222 209 relatively cloud-free images that provided us with coverage of the study area

223 approximately every 2 months from April 1984 to September 2009
224 (http://glovis.usgs.gov/).

225 The following describes the automated classification process that we developed in
226 order to consistently and efficiently transform these 209 images into maps of kelp canopy
227 biomass. First, a single orthorectified TM image was atmospherically corrected to
228 apparent surface reflectance using an atmospheric transmission model (MODTRAN4;
229 Berk et al. 1998). We used this corrected image as a reference and standardized the
230 radiometric signals from all other images to this reference using 50 targets that were
231 assumed to be spectrally stable across the time series (i.e. airport runways, highways,
232 sand dunes, lakes; Furby & Campbell 2001, Baugh & Groeneveld 2008). Outliers were
233 manually removed to reduce the effects of temporal changes in some of these targets.
234 This 'target matching' procedure accounted for all atmospheric, sensor, and processing
235 differences between the scenes and created a time-series of standardized TM imagery.

236 We estimated kelp canopy abundance from the calibrated TM reflectance data
237 using multiple endmember spectral mixture analysis (MESMA). Spectral mixture
238 analysis models the fractional cover of two or more "endmembers" within a pixel. Each
239 endmember represents a pure cover type, and endmembers are assumed to combine
240 linearly (Adams et al., 1993). Standard spectral mixture analysis uses a uniform set of
241 endmembers for the entire image. One challenge in the near-shore marine zone is that the
242 "water" reflectance is influenced by sun glint, breaking surface waves, phytoplankton
243 blooms, dissolved organic matter, sediment runoff, etc. Since water reflectance is highly
244 variable in space and time, a single water endmember cannot be used (Figure 2A).

245 Roberts et al. (1998) developed MESMA to allow endmembers to vary on a per-pixel
246 basis. By selecting from multiple endmembers for one or more cover types, MESMA can
247 better capture the spectral variability of the cover type within an image and through time.
248 MESMA has been extensively used for mapping terrestrial vegetation, include aridland
249 vegetation (Okin et al., 2001), shrublands (Dennison and Roberts, 2003a), forests
250 (Youngentob et al., *in review*), and salt marsh (Li et al., 2005).

251 We modeled pixel reflectance as the linear mixture of reflectance from two
252 endmembers: kelp and water. Thirty water endmembers were selected from non-kelp
253 covered areas within each TM scene using the endmember selection technique described
254 by Dennison and Roberts (2003b). A single kelp endmember was selected by extracting
255 kelp-covered pixel spectra from each image and finding the single spectrum that fit the
256 entire library of kelp spectra with the lowest root mean square error (RMSE) (Dennison
257 and Roberts, 2003b). The pixels in each TM image were then modeled as a two-
258 endmember mixture of kelp and each of the 30 water endmembers. The final model (out
259 of 30) chosen for each pixel was the model that minimized RMSE when fit to the
260 spectrum of that pixel. The result of this process was a measure of the relative fraction of
261 each pixel that was covered by kelp canopy (Figure 2B). We used a kelp fraction
262 threshold of 0.15 to automate the identification of 'kelp-covered' pixels. The multiple
263 endmember process successfully delineated kelp canopy extent under a variety of
264 conditions. Figure 2 provides examples of how our technique retrieved kelp fractions
265 from images that were contaminated by large amounts of sediment runoff (Feb 23, 2005)
266 and high levels of sun glint (July 4, 2006).

267 The retrieved kelp fractions were then compared to giant kelp canopy biomass
268 observations that were collected by divers at permanent plots maintained by the Santa
269 Barbara Coastal Long Term Ecological Research (SBC LTER) project at the Arroyo
270 Quemado and Mohawk kelp forests (Figure 1). The data and the methods used to
271 measure giant kelp canopy biomass from diver surveys are described in detail in
272 Rassweiler et al. (2008). Briefly, divers measured the length of all fronds along 5
273 transects (40 x 1 m) within a plot (40 x 40 m) and converted these lengths to biomass
274 using validated length to weight regressions. Each plot was overlapped by four 30 m TM
275 pixels. For each TM image, we compared the mean kelp fraction of these pixels to the
276 diver measured canopy biomass of each plot with a linear regression.

277 **Regional physical and climate datasets**

278 Pearson correlation coefficients between the satellite-derived time series of
279 regional kelp canopy biomass and physical and climate data that represented first order
280 controls of growth (temperature and nutrients) and disturbance (waves) were calculated
281 on both seasonal and interannual timescales. Kelp canopy biomass was square root
282 transformed to meet assumptions of normality. SST was used as a proxy for ambient
283 nitrate concentrations to investigate the effect of nutrient availability on growth and
284 mortality. Temperature and nitrate are strongly inversely correlated in this region
285 (McPhee-Shaw et al. 2007, Fram et al. 2008). Hourly SST measurements were collected
286 from the National Data Buoy Center's Pt. Arguello buoy for 1984-2009 (Figure 1). The
287 Pt. Arguello buoy is located west of the Santa Barbara Channel and north of Pt.
288 Conception. While generally relatively cool and nutrient rich compared to the rest of the
289 region, this part of our study area captures the temporal variability of the entire region.

290 Otero and Siegel (2004) performed temporal principal components analysis on 4 years
291 (October 1997-June 2001) of satellite-derived SST within our study area and found that
292 91% of the temporal variance was explained by the first mode of variability, which was
293 positively correlated with all parts of the study area. Hence, a single point measurement
294 of SST should be a reliable indicator of the regional temporal variability in SST and, by
295 extension, nutrient concentations.

296 Significant wave height observations were acquired from the National Data Buoy
297 Center's Harvest buoy and Harvest platform sites (Figure 1). The Harvest platform
298 measured significant wave height every 3 hours from January 1987 to April 1999 and the
299 Harvest buoy has collected data two times an hour from March 1998 to the present. We
300 combined these datasets to create a single time series of daily mean significant wave
301 height from 1987-2009, using the Harvest buoy data when both the buoy and platform
302 were operational. Overlapping data from the two were nearly identical (regression slope
303 = 0.96, bias = 0.18, r^2 = 0.97). Both the Harvest buoy and Harvest platform were located
304 west of the Santa Barbara Channel in offshore locations exposed to long-period northwest
305 and south swells. Giant kelp is predominantly affected by extreme wave events (Gaines
306 & Denny 1993, Utter & Denny 1996) and powerful, long-period swell (> 12 seconds) is
307 more important than short-period sea in causing kelp mortality. Since long-period swell
308 affects the entire Channel, we accepted a point measurement as an accurate
309 characterization of the regional wave environment with the understanding that there
310 would be significant spatial variability in the size of breaking waves for a given swell.
311 Currently there is no spatially explicit dataset of nearshore wave heights that matches the
312 spatial resolution and temporal extent of our kelp data. The nearshore wave models that

313 do exist for the Santa Barbara Channel are parameterized using the same Harvest buoy
314 data we used in this study (the Coastal Data Information Project's swell model:
315 http://cdip.ucsd.edu).

316 The Harvest buoy collects wave direction as well as height and period. For the period
317 that the Harvest buoy was operational (1998-present), seasonal histograms of wave
318 direction were calculated for all swell events with periods >= 12 seconds in order to
319 capture the seasonal variability in swell direction. The directional data were used to
320 identify sections of the coast that represented strong gradients in wave exposure.

321 The kelp time series was also compared to the indices of three climate cycles
322 known to affect oceanographic conditions in the Santa Barbara Channel: the Southern
323 Oscillation Index or SOI (http://www.cpc.noaa.gov/data/indices/soi), the Pacific Decadal
324 Oscillation or PDO (http://jisao.washington.edu/pdo/), and the North Pacific Gyre
325 Oscillation or NPGO (http://www.o3d.org/npgo/data/NPGO.txt). By convention,
326 positive anomalies in the PDO represent warmer, nutrient poor conditions in the Santa
327 Barbara Channel while positive anomalies in the SOI and NPGO represent increased
328 upwelling, nutrient, and chlorophyll-a levels. We reversed the sign of the SOI and
329 NPGO for all figures and analyses so that positive deviations in all climate indices
330 represent warmer, nutrient poor conditions.

331 **Subregional dynamics**

332 Spatial heterogeneity in the responses of local kelp populations to regional
333 physical forcings cannot be captured by a regional comparison. Clustering analysis was
334 used to understand how the relationships between physical variables and kelp canopy

335 dynamics varied in space. First, the coastline was divided into 1 km segments and each
336 pixel of kelp canopy was assigned to the closest coastline segment. Segments where kelp
337 did not appear in at least 25% of the images were removed from analysis. Because the
338 amount of kelp in each coastline segment varied from segment to segment, the 1-km
339 segment biomass values were standardized as the proportion of that segment's maximum
340 biomass over the entire time series. The data were then normalized across segments by
341 subtracting the regional mean and dividing by the regional standard deviation of each
342 date. Each segment's degree of wave exposure was calculated using an exposure index
343 based on Baardseth (1970). A circle with a radius of 100 km was placed at the center of
344 each 1 km section of coastline and divided into 40 sectors, each of which had an angle of
345 9°. Sectors were given a score of 0 if they intersected land and 1 if they were free of
346 land. The exposure index is the sum of sector scores; 0 represents complete shelter and
347 40 represents maximum exposure.

348 K-means clustering was used to identify subregions with similar temporal
349 dynamics (e.g. Huth 1996). K-means classification is an unsupervised classification
350 technique that requires the number of clusters to be specified beforehand. The data were
351 clustered using 2-7 clusters to examine the robustness of the results. The kelp canopy
352 biomass of each subregion was then compared to the physical and climate data described
353 above.

354

355 # RESULTS

356 **LANDSAT estimation of kelp canopy biomass**

A strong positive linear relationship was found between the LANDSAT derived kelp fraction index and giant kelp canopy biomass ($r^2 = 0.64$, $p << 0.001$, $df = 94$; Figure 3). We restricted our comparisons to canopy biomass rather than total biomass because optical remote sensing only detects floating kelp. Generally canopy biomass is highly correlated to total biomass ($r^2 = 0.92$; unpublished SBC LTER data); however, the relationship between TM kelp fraction and canopy biomass was stronger than between kelp fraction and total biomass ($r^2 = 0.49$, $p << 0.001$, $df = 94$). This discrepancy was driven by a few data points where the ratio of canopy to total biomass was unusually low. Neither tidal nor current fluctuations had any effect on the kelp fraction/canopy biomass relationship ($p = 0.65$ and 0.25 when the residuals of the fraction-biomass relationship were compared to local tides and currents for the time of LANDSAT data collection, respectively). This result agrees with previous work showing that the relatively weak tidal fluctuations and current speeds in this area do not affect remote sensing estimates of kelp biomass as they do in other locations (Cavanaugh et al. 2010 compared to Britton-Simmons et al. 2008). The relationship between satellite derived kelp fraction and diver measured canopy biomass (Figure 3) was used to transform images of kelp fractional cover into quantitative, validated maps of giant kelp canopy biomass. These maps are available every 1 to 2 months for the past 25 years and resolve giant kelp canopy biomass on spatial scales of 30 m to regional scales, which is here defined as the extent of the LANDSAT 5 TM scene used (Figure 1).

Regional dynamics

The regionally averaged giant kelp canopy biomass is shown in Figure 4A. The long-term (1984-2009) mean regional giant kelp canopy biomass was 43,700 wet metric

tons but there was an extremely high amount of variability about this mean, as evidenced by a temporal coefficient of variation of 86%. Changes in regional kelp biomass were rapid and order of magnitude increases and decreases in regional mean biomass routinely occurred over a span of less than 4 months. Most years displayed a seasonal cycle with biomass minimums occurring in the winter followed by rapid growth in the spring and early summer leading to maximums in late summer or early fall; however, the amplitude and timing of this cycle varied substantially. This seasonal cycle was superimposed on a cycle with a 12-13 year period. In this longer cycle relatively low periods of canopy biomass in 1984-1990 and 1994-2003 were separated by high biomass periods in 1990-1995 and 2003-2009. The length of this cycle matches the 11-13 year period of the NPGO (Figure 4A; Di Lorenzo et al 2008). We plotted the kelp and NPGO time series together in Figure 4A to emphasize this match in periods and to facilitate the interpretation of Figures 4 A & D. There were no long-term trends in the regional canopy biomass time series.

Both SST and wave height displayed the pronounced seasonal cycles characteristic of this region (Figure 4B and 4C). SST typically reached its annual minimum between February and March and its maximum between August and October. Significant wave height maximums occurred in the winter months, corresponding with the timing of increased storm activity in the North Pacific. Between 1987 and 2009 the annual maximum winter (Dec.-Feb.) wave height averaged 4.9 m while the annual maximum summer (June-Aug.) wave height averaged 3.26 m. During our study period annual mean significant wave heights increased significantly at the pace of 0.02 m yr^{-1} ($F_{1,22} = 25.9$, $p < 0.001$). This positive trend in wave height agrees with other

403 observations of increasing wave heights in the Northeast Pacific over the last 60 years
404 (Bromirski et al. 2003, Ruggiero et al. 2010).

405 The oscillations of the three climate cycles ranged from 3-7 years (SOI) to 11-13
406 years (NPGO) to 20-30 years (PDO) (Figure 4 A & D). All climate indices experienced
407 both positive and negative extremes during our study period. The 1990s saw a number of
408 positive El Niño anomalies and the 1997-1998 El Niño was one the strongest ever
409 recorded. La Niña conditions were present in 1998-1999, 2001, and 2008. The NPGO
410 cycled fairly consistently with positive (nutrient poor) anomalies in the early 1990s and
411 mid 2000s separated by negative anomalies in the early 2000s. The PDO displayed
412 mostly positive anomalies from the beginning of the time series until the early to mid
413 2000s when negative anomalies became more prevalent; this change may represent a shift
414 of the PDO from the warm phase that began in the late 1970s (Mantua et al. 1997,
415 Peterson and Schwing 2003). All climate indices were positively correlated with SST
416 (Table 1). The NPGO was weakly negatively correlated with higher wave heights; there
417 was no significant relationship between either SOI or PDO and waves.

418 *Seasonal relationships to physical and climate variables*

419 We examined the relationships between physical and climate variables and
420 monthly variability in kelp biomass by calculating Pearson correlation coefficients
421 between square root normalized regional kelp canopy biomass and each of the physical
422 and climate variables. Univariate correlation analyses indicated that there were
423 significant but weak negative relationships between kelp canopy biomass and both SST
424 and wave height on monthly timescales (Table 1). The failure of SST and wave height to

425 explain much variation in kelp canopy biomass at this scale is not surprising given the
426 high level of month-to-month variability in the kelp time series as well as the large spatial
427 scale over which regional kelp biomass was evaluated. The PDO was the only climate
428 index with a significant correlation to kelp biomass, however the relationship was again
429 weak. While the SOI index was not significantly correlated with kelp biomass, strong El
430 Niño events in the winters of 1997-1998 and 2002-2003 corresponded with massive
431 regional kelp canopy losses (regional kelp biomass dropped to almost zero). In addition,
432 strong La Niña events in late 1988 and 2008 marked large increases in regional kelp
433 biomass.

434 We further investigated the relationship between physical forcings and seasonal
435 kelp variability by isolating winter canopy losses and spring recoveries and comparing
436 them to our physical forcing variables. Winter loss was defined as the percent change in
437 regional kelp canopy biomass from the fall (Aug-Nov) maximum to the winter (Dec-
438 March) minimum of each year; the specific time frame varied from year to year
439 depending on the timing of kelp maximums and minimums. We compared the percent
440 loss of kelp to the maximum wave height over the same time period and found a strong
441 polynomial relationship between the two that appeared to saturate between wave heights
442 of 6-7 m (Figure 5A). Only the extreme wave events appeared to control regional kelp
443 biomass, we did not find significant relationships between waves and kelp losses for
444 other times of the year when waves were smaller. There was no significant relationship
445 between winter loss and nutrient levels ($r^2 = 0.00$, $p = 0.75$). Among the climate indices
446 we found a weak but significant positive relationships between winter PDO and kelp loss

447 ($r^2 = 0.19$, $p = 0.03$) and between winter SOI and kelp loss ($r^2 = 0.16$, $p = 0.05$) but no
448 significant relationship between NPGO and kelp loss ($r^2 = 0.05$, $p = 0.31$).

449 A similar analysis was performed between spring recovery and nutrient levels.
450 Spring recovery was defined as the increase in canopy biomass between the winter (Dec-
451 March) minimum and the spring/summer (April-July) maximum of each year. Biomass
452 increases were log transformed to meet assumptions of normality for the linear
453 regression. There was a weaker (as compared to kelp loss vs. waves), but still highly
454 significant negative linear relationship between spring/summer recovery of regional kelp
455 biomass and mean SST (Figure 5B). There was no significant relationship between
456 spring recovery and wave heights or any of the climate indices.

457 *Interannual relationships to physical and climate variables*

458 To investigate the drivers of interannual variability in kelp canopy biomass we
459 calculated the cross correlation, at lags of 0-6 years, of annual mean canopy biomass and
460 the annual means of SST, and the 3 climate indices, and annual maximums of significant
461 wave height. On interannual timescales there was no direct significant relationship
462 between annual mean kelp canopy biomass and any of the physical or climate variables
463 (Table 1B). However, cross correlation analysis revealed strong and significant 3-year
464 lagged relationships between kelp canopy biomass and SST, waves, and NPGO ($r = -$
465 0.48, 0.48, and -0.50 respectively; Figure 6). There was no significant relationship
466 between kelp canopy biomass and SOI or PDO at any lag.

467 **Subregional dynamics**

468 The clustering analysis divided the Santa Barbara Channel into subregions along
469 wave exposure and nutrient gradients. The clustering results were robust to varying the
470 number of clusters used in the k-means algorithm: all solutions separated the mainland
471 coastline at Pt. Conception and separated the north and south sides of the Channel
472 Islands. We displayed the results from the 4-group clustering in Figure 7; increasing the
473 number of clusters simply further separated these 4 'major' subregions into smaller
474 groups. The subregions from the 4-cluster solution were labeled A to D in order of
475 decreasing mean exposure as measured by the exposure index (Table 2). Bonferroni
476 adjusted paired t-tests demonstrated that the mean exposures of the two 'exposed'
477 subregions (A and B) were not significantly different from each other, but each was
478 significantly different from the two 'sheltered' regions (C and D) ($p<0.01$). It is
479 important to note that the exposure index measures potential exposure, it does not take
480 into account the direction of swells. Because the largest swells in the Santa Barbara
481 Channel come from the northwest (Figure 7), the index may overestimate the realized
482 exposure of regions that are sheltered from northwest swells, but exposed to swells from
483 other directions (i.e. subregion B).

484 Temporal dynamics of the four subregions were relatively similar (mean pairwise
485 $r = 0.61$, Figure 8); however, upon closer inspection it was possible to identify
486 differences that tracked wave exposure. Kelp canopy biomass dynamics of the exposed
487 subregions were well correlated to maximum wave heights, but not SST, while the
488 dynamics of sheltered subregions corresponded to SST, but not wave heights (Table 2).
489 In addition, the strength of seasonal cycles increased with increasing exposure (Figure 9).
490 As the strength of the seasonal cycle decreased with decreasing exposure, the strength of

491 the longer 12-13 year period cycle increased, suggesting a closer connection between the
492 NPGO and sheltered regions (Figure 8). For example, the extended periods of low
493 regional canopy biomass in 1984-1990 and 1994-2003 reflected a near complete lack of
494 recovery in the sheltered regions; the exposed regions maintained relatively high levels of
495 biomass during these years.

496

497 # DISCUSSION

498 **Remote sensing of kelp forests**

499 Our LANDSAT 5 TM dataset represents the first high resolution, local- to
500 regional-scale assessment of giant kelp canopy biomass on monthly to decadal
501 timescales. This dataset is itself a significant accomplishment as it provides a novel view
502 into kelp forest dynamics across a wide range of scales. Previous studies have
503 demonstrated the feasibility of measuring kelp canopy cover and biomass with aerial and
504 satellite imagery (Jensen et al. 1980, Deysher 1993, Stekoll et al. 2006, Cavanaugh et al.
505 2010); however these studies have not had the extended temporal coverage that is
506 presented here. Recent work by Parnell et al. (2010) examined annual to decadal
507 variability in giant kelp cover near San Diego using aerial surveys, but they used annual
508 kelp maximums and so did not measure seasonal variability. While LANDSAT provides
509 unmatched temporal resolution and coverage, it has a coarser spatial resolution than the
510 sensors used in some of these previous studies (30 m as compared to ~1 m in Stekoll et
511 al. 2006 and 10 m in Cavanaugh et al. 2010). In addition, LANDSAT has a relatively
512 low radiometric resolution; this limits the ability of the sensor to differentiate small

changes in reflectance between pixels. One consequence of the reduced spatial and radiometric resolution of LANDSAT is higher levels of uncertainty when comparing satellite data to transect scale diver-measured biomass (the r^2 between LANDSAT and diver measured canopy biomass was 0.64 compared to 0.77 for Cavanaugh et al. 2010 and 0.84 for Stekoll et al. 2006). Nevertheless, the LANDSAT-canopy biomass relationship was still strong and highly significant and provides a path for assessing regional satellite canopy biomass variations. As the availability of imagery with higher spatial and radiometric resolutions increases, more accurate remotely sensed time series of kelp can be developed using techniques similar to the one we have presented here.

Regional dynamics

Recently, investigators have speculated that the global extent of kelp forests is shrinking (i.e. Hoegh-Guldberg and Bruno 2010). We did not find a significant negative long-term trend in the 25-year record of kelp canopy biomass of the Santa Barbara Channel. Long-term trends in giant kelp are difficult to identify because canopy biomass varies across orders of magnitude over short time periods. Large disturbance events (i.e. strong El Niños) cause dramatic large-scale reductions in canopy biomass, however recoveries can be almost as rapid. There is an upper limit on the amount of kelp that the region can support that is based simply on the availability of suitable habitat. However, it seems difficult to identify a regional equilibrium for giant kelp canopy due to its highly dynamic nature. If the global extent of kelp is indeed shrinking, then it will likely be difficult to detect in regions such as the Santa Barbara Channel that are at the center of giant kelp's hemispherical range. While we did not observe a long-term directional trend in kelp canopy biomass, we did find that regional scale kelp biomass oscillated on cycles

536 with periods of 1 and 12-13 years. The annual cycles were related to winter storm
537 activity and, to a lesser extent, nutrient levels (Figure 5). While physical storm driven
538 mortality was direct and immediate, the effect of nutrients on kelp growth were likely
539 delayed and complicated by a number of other factors including the availability of light
540 and space, spore settlement and recruitment, etc.; hence, a weaker relationship was
541 observed. In addition, variability in the nutrient/temperature relationship may propagate
542 to our attempts at relating nutrient levels to biomass dynamics. While these winter losses
543 and spring recoveries characterized the annual cycle in general there was a great deal of
544 variability in the amplitude and timing of these cycles from year to year.

545 Interannual relationships between kelp canopy biomass and physical drivers were
546 less clear. Recovery of kelp populations can be extremely rapid and so annual means and
547 maximums can be decoupled from the previous winter's wave disturbance. This may
548 help explain why past studies using annual observations made in the summer or fall failed
549 to find a relationship between waves and kelp population metrics (Tegner et al. 1996).
550 The longer period cycles in kelp biomass corresponded to the NPGO, waves, and nutrient
551 levels (as inferred from SST), but lagged these variables by 3 years (Figure 6). This 3-
552 year lag is somewhat counterintuitive in light of the rapid turnover of the fronds that
553 create kelp canopies. We suspect that the lagged relationships are related to plant level
554 recruitment and mortality. While losses at the frond level occur continuously throughout
555 the year, mortality of entire plants occurs more episodically and is related to large wave
556 events (Reed et al. 2008). Exceptionally large wave events can clear space and allow for
557 dramatic spikes in recruitment (Graham et al. 1997). Previous work has shown that
558 environmental conditions at the time of recruitment and juvenile growth of kelp cohorts

559 can have long lasting effects on population dynamics and community structure (Tegner et
560 al. 1997, Dayton et al. 1999). For example, Tegner et al. (1997) compared succession
561 after 2 large disturbances under contrasting oceanographic regimes and found that
562 nutrient rich conditions led to high densities and competitive dominance of giant kelp that
563 lasted for the life of the cohort. This result agrees with the lagged negative relationship
564 we found between nutrient levels and kelp canopy biomass. Together, large waves and
565 high nutrient levels in a given year allow for the recruitment and juvenile growth of a
566 new cohort of giant kelp plants (Figure 10). This cohort matures over the next 2-3 years,
567 developing high levels of canopy biomass in the absence of severe storms. Currently, in
568 Southern California severe storms occur at the average frequency of 1 every 3.5 years
569 (Graham et al. 1997), thus allowing populations to expand their areal extents until the
570 cycle is repeated or all available habitat is utilized. In addition, LANDSAT only
571 measures canopy changes; it takes approximately 6-8 months for a newly recruited kelp
572 plant to reach the surface (author's personal obervations) and so there is an inherent lag
573 in responses observed with satellite imagery.

574 Many studies have linked massive declines in kelp populations to severe El Niño
575 conditions and have observed rapid recovery of kelp populations during nutrient rich La
576 Niña events (Dayton and Tegner 1989, Dayton 1992, 1999, Edwards 2004). In addition,
577 Parnell et al. (2010) found that the response of kelp populations to El Niño events is
578 modulated by low frequency changes in the PDO: the importance of nutrient control in
579 the San Diego area increased after the PDO switched to a warm phase in the late 1970s.
580 However, the relationship between kelp and the NPGO has largely been neglected. We
581 observed that strong El Niño events in 1987, 1997, and 2003 coincided with large

582 regional mortality events (Figure 4); however, the long (12-13 year) period cycles in
583 regional kelp biomass were better correlated with the NPGO, again at a 3 year lag. The
584 NPGO is driven by regional variations in wind-driven upwelling and horizontal advection
585 and corresponds closely with correlates of ecosystem productivity such as nutrient levels
586 and chlorophyll concentrations (Di Lorenzo et al. 2008). Therefore, the NPGO appears
587 to influence decadal variations in kelp canopy biomass though large-scale, low frequency
588 changes in nutrient availability that in turn affect recruitment and growth of kelp
589 populations.

590 While no long-term trends were evident in the kelp time series, we did see a
591 significant long-term increase in mean and maximum wave heights over our study period.
592 Other studies have observed similar trends in the Eastern Pacific (Bromirski et al. 2003,
593 Ruggiero et al. 2010) and many climate models predict that the frequency, and possibly
594 the intensity of large storms will continue to increase in this region (Easterling et al.
595 2000, Meehl et al. 2000, Meehl et al. 2007). This has the potential to increase the effects
596 of wave events on the more sheltered coastlines of southern California, leading to higher
597 annual winter losses. Reed et al (2008) found that biomass at the start of the growth year
598 (after winter storm disturbances) explained 63% of the observed variation in annual net
599 primary productivity of three kelp populations in the Santa Barbara Channel . Therefore,
600 increased wave losses would likely lead to decreased productivity by giant kelp in this
601 region . In addition, the implications of increased levels of physical disturbance span
602 trophic levels as repeated kelp loss due to waves has been linked to lower diversity and
603 complexity of kelp forest food webs (Byrnes et al. in review).

604 **Subregional dynamics**

605 The Santa Barbara Channel experiences a large amount of spatial variability in
606 environmental conditions. As a result, the regional comparison of kelp biomass to
607 physical variables may be confounded by the response of subregions that are controlled
608 by different physical forcings. We found that subregions with similar temporal dynamics
609 could be separated statistically and these subregions have different wave exposures and
610 respond differently to variations in SST and presumably nutrient levels (Table 2). The
611 dynamics of the relatively sheltered mainland coastline south of Pt. Conception
612 (subregion D) were significantly correlated with SST, but not maximum wave height.
613 Tegner et al. (1996) observed similar behavior in the Pt. Loma kelp forest near San
614 Diego: a measure of canopy density was significantly correlated with SST but not wave
615 heights. Also, in many years minimum canopy biomass levels occurred in late
616 summer/early fall for subregion D (Figure 9). This is generally a time of relatively low
617 wave energy and low nutrient levels, suggesting that senescence unrelated to waves is
618 causing these annual minimums.

619 Our results indicate that Pt. Conception marks a major biogeographic boundary
620 for the dynamics of giant kelp forests in California. Changes in kelp biomass along the
621 exposed coastline north of Pt. Conception were well correlated with wave height, but not
622 SST as high storm mortalities were observed each winter. This created a pronounced and
623 predictable seasonal cycle with lower interannual variability than the more sheltered
624 subregions to the south (Figure 9). The high variation in canopy biomass observed in
625 October and November (e.g. long boxes in Figure 9A) reflect variability in the timing of
626 the onset of the winter storm season. Relatively high nutrient conditions in this subregion
627 likely allowed for consistent spring recovery each year (Jackson 1987). This result

628 agrees with a study by Donnellan (2004) that found that seasonal canopy dynamics of
629 exposed Central Californian kelp beds were highly regular and predictable. The
630 subregions containing the Channel Islands represented a combination of more complex
631 exposures. Subregion B displayed dynamics similar to the exposed subregion A even
632 though subregion B was protected from large northwest swells. This likely reflects the
633 fact that both subregions are rarely nutrient limited and so nutrient fluctuations have less
634 control on biomass dynamics in these regions. Like the coastline north of Point
635 Conception, the south sides of the two westernmost Channel Islands are typically bathed
636 in cold, nutrient-rich upwelled water (Harms and Winant 1998; Otero and Siegel, 2004).

637 Previous local empirical and theoretical studies have observed kelp populations
638 fluctuating on cycles of 3-5 years and have theorized that these fluctuations are due to
639 seasonal forcings such as wave disturbance. Graham et al. (1997) found these cycles in
640 both exposed kelp populations of central California as well as more sheltered populations
641 of southern California. Their work suggested that in sheltered populations recruitment
642 occurred continuously and so the cycles were controlled by the irregularity of large storm
643 events. In exposed populations where large storms occurred more frequently, sporadic
644 recruitment created a lag in recovery that was dependent on the coincidence of a juvenile
645 population and conditions suitable for juvenile growth. Such lags in recovery can cause
646 interannual cycling. Nisbet and Bence (1989) developed a family of 2-stage kelp
647 population models (juvenile and adults) that reproduced similar 3-5 year cycles as well as
648 more regular annual cycles. Their models were based on the idea that population
649 dynamics are driven by recruitment events which are in turn controlled by temperature,
650 bottom irradiance, and unknown stochastic factors. Their models predicted that larger

651 seasonal fluctuations in surface irradiance and adult mortality, such as those that occur in
652 central California, should lead to more regular annual recruitment. On a regional scale,
653 we found that 3-5 year cycles were much more evident in sheltered subregions than in
654 exposed regions (compare subregion A to subregion D in Figure 8). Exposed coastlines
655 experienced regular annual cycles of winter mortality and spring recovery. The increased
656 regularity of the annual cycles we observed compared to those observed by Graham et al.
657 (1997) in central California may have been due to the difference in the spatial scales of
658 our studies. In exposed regions, recovery lags that produce irregular cycles at local scales
659 (as in Graham et al. 1997) may be averaged out at the regional scale. A regional cycle
660 will be apparent if mortality is consistent across the entire region and enough local
661 populations recover each year.

662 Long-term time series data from sensors such as LANDSAT is becoming
663 increasingly available at little to no cost. While the benefits of increased spatial coverage
664 have been well recognized, the temporal coverage of these datasets has been under-
665 utilized. Given the time and costs involved in collecting field data in situ there is great
666 potential for satellite data such as LANDSAT to provide much needed insight into the
667 patterns and controls of dynamic systems like giant kelp forests over large spatial and
668 long temporal scales.

669

670 **Acknowledgements**

671 The authors would like to acknowledge the support of NASA Interdisciplinary
672 Science program and the National Science Foundation's support of the Santa Barbara

673 Coastal Long-Term Ecological Research site. K Cavanaugh would like to acknowledge
674 support from the NASA Earth System Science fellowship program.

675

675

676 **LITERATURE CITED**

677 Adams J, Smith M, Gillespie A (1993) Imaging spectroscopy: Interpretation based on spectral
678 mixture analysis. Remote geochemical analysis: Elemental and mineralogical
679 composition 7:145 – 166

680 Adams P, Inman D, Graham N (2008) Southern California Deep-Water Wave Climate:
681 Characterization and Application to Coastal Processes. Journal of Coastal Research
682 24:1022-1035

683 Baardseth E (1970) A square-scanning, two stage sampling method of estimating seaweed
684 quantities. Rep Norw Inst Seaweed Res 33:1 – 41

685 Barber R, Chavez F (1983) Biological consequences of El Niño. Science 222:1203-1210

686 Baugh W, Groeneveld D (2008) Empirical proof of the empirical line. International Journal of
687 Remote Sensing 29:665-672

688 Behrenfeld M, O' Malley R, Siegel D, McClain C, Sarmiento J, Feldman G, Milligan A,
689 Falkowski P, Letelier R, Boss E (2006) Climate-driven trends in contemporary ocean
690 productivity. Nature 444:752-755

691 Berk A, Bernstein LS, Anderson GP, Acharya PK, Robertson DC, Chetwynd JH, Adler-Golden
692 SM (1998) MODTRAN Cloud and Multiple Scattering Upgrades with Application to
693 AVIRIS - editions of 1991 and 1992. Remote Sensing of Environment 65:367-375

694 Britton-Simmons K, Eckman J, Duggins D (2008) Effect of tidal currents and tidal stage on
695 estimates of bed size in the kelp Nereocystis luetkeana. Marine Ecology-Progress Series
696 355:95

697 Bromirski P, Flick R, Cayan D (2003) Storminess variability along the California coast: 1858-
698 2000. Journal of Climate 16:982-993

699 Byrnes J, Reed D, Cardinale B, Cavanaugh K, Holbrook S, Schmitt R (in review) Climate
700 Driven Increases in Storm Frequency Simplify Kelp Forest Food Webs. Global Change
701 Biology

Cavanaugh K, Siegel D, Kinlan B, Reed D (2010) Scaling giant kelp field measurements to regional scales using satellite observations. Marine Ecology Progress Series 403:13-27

Change IPoC, (IPCC) (2007a) Climate change 2007: impacts, adaptation and vulnerability. IPCC, Geneva, Switzerland

Dayton, P.K., Currie, V., Gerrodette, T., Keller, B.D., Rosenthal, R.J. & Van Tresca, D. 1984. Patch dynamics and stability of some California kelp communities. Ecological Monographs 54, 253–289.

Dayton P, Tegner M, Edwards P, Riser K (1999) Temporal and spatial scales of kelp demography: the role of oceanographic climate. Ecological Monographs 69:219-250

Dayton PK, Tegner MJ (1990) Bottoms beneath troubled waters: benthic impacts of the 1982-1984 El Niño in the temperature zone. Elsevier oceanography series 52:433-472

Dayton PK, Tegner MJ, Parnell PE, Edwards PB (1992) Temporal and spatial patterns of disturbance and recovery in a kelp forest community. Ecological Monographs 62:421-445

Dennison P and Roberts D (2003a) The effects of vegetation phenology on endmember selection and species mapping in southern California chaparral. Remote Sensing of Environment 87:295-309

Dennison P, Roberts D (2003b) Endmember selection for multiple endmember spectral mixture analysis using endmember average RMSE. Remote Sensing of Environment 87:123-135

Deysher, L.E. & Dean, T.A. 1986b. *In situ* recruitment of sporophytes of the giant kelp *Macrocystis pyrifera* (L.) C.A. Agardh: effects of physical factors. Journal of Experimental Marine Biology and Ecology 103, 41–63.

Deysher LE (1993) Evaluation of remote sensing techniques for monitoring giant kelp populations. Hydrobiologia 261:307-312

Di Lorenzo E, Schneider N, Cobb K, Franks P, Chhak K, Miller A, McWilliams J, Bograd S, Arango H, Curchitser E (2008) North Pacific Gyre Oscillation links ocean climate and ecosystem change. Geophys Res Lett 35:6

Di Lorenzo E, Schneider N, Cobb K, Furtado J, Alexander M (2009) ENSO and the North

730 Pacific Gyre Oscillation: an integrated view of Pacific decadal dynamics. Geophysical
731 Research Letters, submitted

732 Doney S, Fabry V, Feely R, Kleypas J (2009) Ocean acidification: the other CO2 problem.
733 Marine Science 1

734 Donnellan M (2004) Spatial and temporal variability of kelp forest canopies in central California.
735 San Jose State University

736 Easterling D, Meehl G, Parmesan C, Changnon S, Karl T, Mearns L (2000) Climate extremes:
737 observations, modeling, and impacts. Science 289:2068

738 Edwards MS (2004) Estimating scale-dependency in disturbance impacts: El Niños and giant
739 kelp forests in the northeast Pacific. Oecologia 138:436-447

740 Foster M, Schiel D (1985) Ecology of giant kelp forests in California: A community profile,
741 FWS/OBS-85 (7.2), San Jose State Univ., Moss Landing, CA (USA). Moss Landing
742 Marine Labs.

743 Fram J, Stewart H, Brzezinski M, Gaylord B, Reed D, Williams S, MacIntyre S (2008) Physical
744 pathways and utilization of nitrate supply to the giant kelp, Macrocystis pyrifera.
745 Limnology and Oceanography 53:1589-1603

746 Furby S, Campbell N (2001) Calibrating images from different dates to 'like-value' digital
747 counts. Remote Sensing of Environment 77:186-196

748 Gaines S, Denny M (1993) The largest, smallest, highest, lowest, longest, and shortest: extremes
749 in ecology. Ecology 74:1677-1692

750 Graham M (2004) Effects of local deforestation on the diversity and structure of southern
751 California giant kelp forest food webs. Ecosystems 7:341-357

752 Graham M, Halpern B, Carr M (2008) Diversity and Dynamics of Californian Subtidal Kelp
753 Forests. Food Webs and the Dynamics of Marine Reefs:103

754 Graham M, Vasquez J, Buschmann A (2007) Global ecology of the giant kelp Macrocystis: from
755 ecotypes to ecosystems. Oceanography and Marine Biology: An Annual Review 45:39-
756 88

757 Graham MH, Harrold C, Lisin S, Light K, Watanabe JM, Foster MS (1997) Population dynamics

758 of giant kelp Macrocystis pyrifera along a wave exposure gradient. Marine Ecology-
759 Progress Series 148:269-279

760 Harley C, Randall Hughes A, Hultgren K, Miner B, Sorte C, Thornber C, Rodriguez L, Tomanek
761 L, Williams S (2006) The impacts of climate change in coastal marine systems. Ecology
762 letters 9:228-241

763 Harms S, Winant C (1998a) Characteristic patterns of the circulation in the Santa Barbara
764 Channel. Journal of Geophysical Research 103:3041-3065

765 Harms S, Winant C (1998b) Characteristic patterns of the circulation in the Santa Barbara
766 Channel. Journal of Geophysical Research 103:3041-3065

767 Hickey B (1979) The California current system--hypotheses and facts. Progress in Oceanography
768 8:191-279

769 Hoegh-Guldberg O, Bruno J (2010) The impact of climate change on the world's marine
770 ecosystems. Science 328:1523

771 Huth R (1996) An intercomparison of computer-assisted circulation classification methods.
772 International Journal of Climatology 16:893-922

773 Jackson G (1987) Modelling the growth and harvest yield of the giant kelp Macrocystis pyrifera.
774 Marine Biology 95:611-624

775 Jensen JR, Estes JE, Tinney L (1980) Remote sensing techniques for kelp surveys.
776 Photogrammetric Engineering and Remote Sensing 46:743-755

777 Lee D, Storey J, Choate M, Hayes R (2004) Four years of Landsat-7 on-orbit geometric
778 calibration and performance. IEEE Transactions on Geoscience and Remote Sensing
779 42:2786-2795

780 Levin S (1992) The problem of pattern and scale in ecology: the Robert H. MacArthur award
781 lecture. Ecology 73:1943-1967

782 Li L, Ustin S, Lay M (2005) Application of multiple endmember spectral mixture analysis
783 (MESMA) to AVIRIS imagery for coastal salt marsh mapping: A case study in China
784 Camp, CA, USA. International Journal of Remote Sensing 26:5193-5207

785 Mantua N, Hare S (2002) The Pacific decadal oscillation. Journal of Oceanography 58:35-44

786 Mantua N, Hare S, Zhang Y, Wallace J, Francis R (1997) A Pacific interdecadal climate
787 oscillation with impacts on salmon production. Bulletin of the American Meteorological
788 Society 78:1069-1079

789 Markham B, Storey J, Williams D, Irons J (2004) Landsat sensor performance: history and
790 current status. Geoscience and Remote Sensing, IEEE Transactions on 42:2691-2694

791 McPhee-Shaw EE, Siegel DA, Washburn L, Brzezinski MA, Jones JL, Leydecker A, Melack J
792 (2007) Mechanisms for nutrient delivery to the inner shelf: Observations from the Santa
793 Barbara Channel. Limnology and Oceanography 52:1748-1766

794 Meehl G, Stocker T, Collins W, Friedlingstein P, Gaye A, Gregory J, Kitoh A, Knutti R, Murphy
795 J, Noda A (2007) Global climate projections Climate Change 2007: The Physical Science
796 Basis. Contribution of Working Group I to the Fourth Assessment Report of the
797 Intergovernmental Panel on Climate Change. D Qin, M Manning, Z Chen, M Marquis, K
798 Averyt, M Tignor and HL Miller (New York: Cambridge University Press) pp:747 – 845

799 Meehl G, Zwiers F, Evans J, Knutson T, Mearns L, Whetton P (2000) Trends in extreme weather
800 and climate events: Issues related to modeling extremes in projections of future climate
801 change. Bulletin of the American Meteorological Society 81:427-436

802 Nisbet R, Bence J (1989) Alternative dynamic regimes for canopy-forming kelp: a variant on
803 density-vague population regulation. American Naturalist:377-408

804 O'Reilly W, Guza R (1993) A comparison of two spectral wave models in the Southern
805 California Bight. Coastal Engineering 19:263-282

806 Okin G, Roberts D, Murray B, Okin W (2001) Practical limits on hyperspectral vegetation
807 discrimination in arid and semiarid environments. Remote Sensing of Environment 77:
808 212-225

809 Otero M, Siegel D (2004) Spatial and temporal characteristics of sediment plumes and
810 phytoplankton blooms in the Santa Barbara Channel. Deep Sea Research Part II: Topical
811 Studies in Oceanography 51:1129-1149

812 Parnell PE, Miller EF, Lennert-Cody CE, Dayton PK, Carter ML, Stebbins TD (2010) The
813 response of giant kelp (Macrocystis pyrifera) in southern California to low-frequency

814 climate forcing. Limnology and Oceanography 55(6):2686-2702

815 Przeslawski R, Ahyong S, Byrne M, Woerheide G, Hutchings P (2008) Beyond corals and fish:
816 the effects of climate change on noncoral benthic invertebrates of tropical reefs. Global
817 Change Biology 14:2773-2795

818 Raimondi P, Reed D, Gaylord B, Washburn L (2004) Effects of self-fertilization in the giant
819 kelp, Macrocystis pyrifera. Ecology 85:3267-3276

820 Rassweiler A, Arkema K, Reed D, Zimmerman R, Brzezinski M (2008) Net primary production,
821 growth, and standing crop of Macrocystis pyrifera in southern California. Ecology
822 89:2068-2068

823 Reed D, Neushul M, Ebeling A (1991) Role of settlement density on gametophyte growth and
824 reproduction in the kelps Pterygophora californica and Macrocystis
825 pyrifera(Phaeophyceae). Journal of Phycology 27:361-366

826 Reed D, Rassweiler A, Arkema K (2008) Biomass rather than growth rate determines variation
827 in Net primary production by giant kelp. Ecology 89:2493-2505

828 Reed D, Rassweiler A, Carr M, Cavanaugh K, Malone D, Siegel D (in prep) Wave disturbance
829 overwhelms top-down and bottom-up control of primary production in California kelp
830 forests. Ecology

831 Reed DC, Kinlan BP, Raimondi PT, Washburn L, Gaylord B, Drake PT (2006) A
832 metapopulation perspective on patch dynamics and connectivity of giant kelp. Marine
833 Metapopulations Academic Press, San Diego

834 Roberts D, Gardner M, Church R, Ustin S, Scheer G, Green R (1998) Mapping chaparral in the
835 Santa Monica Mountains using multiple endmember spectral mixture models. Remote
836 Sensing of Environment 65:267-279

837 Rosenzweig C, Karoly D, Vicarelli M, Neofotis P, Wu Q, Casassa G, Menzel A, Root T, Estrella
838 N, Seguin B (2008) Attributing physical and biological impacts to anthropogenic climate
839 change. Nature 453:353-357

840 Ruggiero P, Komar P, Allan J (2010) Increasing wave heights and extreme value projections:
841 The wave climate of the US Pacific Northwest. Coastal Engineering 57:539-552

842 Seymour R (1998) Effects of El Niños on the west coast wave climate. Shore & Beach 66:3-6

843 Smith C, Sardeshmukh P (2000) The effect of ENSO on the intraseasonal variance of surface
844 temperatures in winter. International Journal of Climatology 20:1543-1557

845 Stekoll MS, Deysher LE, Hess M (2006) A remote sensing approach to estimating harvestable
846 kelp biomass. Journal of Applied Phycology 18:323-334

847 Steneck RS, Graham MH, Bourque BJ, Corbett D, Erlandson JM, Estes JA, Tegner MJ (2002)
848 Kelp forest ecosystems: biodiversity, stability, resilience and future. Environmental
849 Conservation 29:436-459

850 Tegner M, Dayton P, Edwards P, Riser K (1996) Is there evidence for long-term climatic change
851 in southern California kelp forests? California Cooperative Oceanic Fisheries
852 Investigations Report:111-126

853 Tegner M, Dayton P, Edwards P, Riser K (1997) Large-scale, low-frequency oceanographic
854 effects on kelp forest succession: a tale of two cohorts. Marine Ecology Progress Series
855 146:117-134

856 Utter B, Denny M (1996) Wave-induced forces on the giant kelp Macrocystis pyrifera (Agardh):
857 field test of a computational model. The Journal of experimental biology 199:2645

858 Youngentob K, Roberts D, Held A, Dennison P, Jia X, Lindenmayer D, Mapping two Eucalyptus
859 subgenera using multiple endmember spectral mixture analysis and continuum-removed
860 imaging spectrometry data. Remote Sensing of Environment, in review, accepted with
861 minor revisions.

862 Zimmerman R, Kremer J (1984) Episodic nutrient supply to a kelp forest ecosystem in Southern
863 California. Journal of Marine Research 42:591-604

864 Zimmerman RC, Kremer JN (1986) In situ growth and chemical-composition of the giant
865 kelp, Macrocystis pyrifera: response to temporal changes in ambient nutrient
866 availability. Marine Ecology-Progress Series 27:277-285

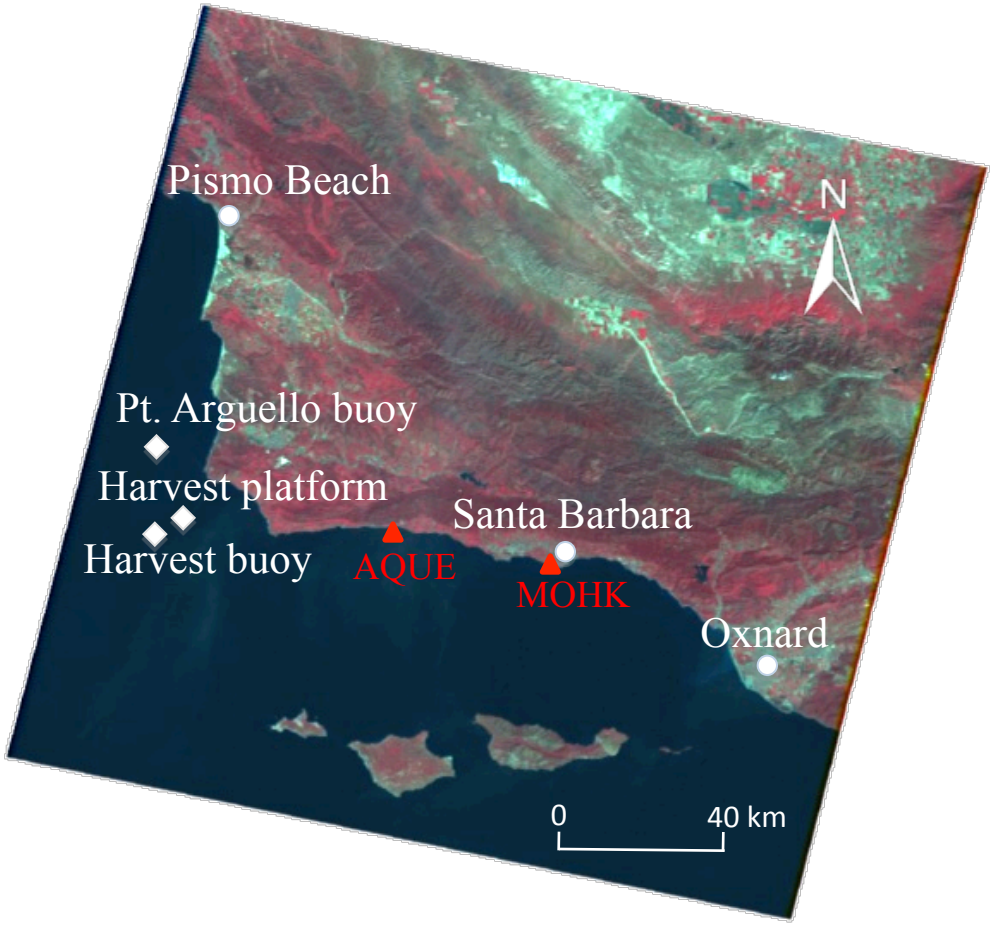

Figure 1. LANDSAT TM scene displaying study area, Pt. Arguello, Harvest, and Harvest Platform buoys, and LTER diver transects at the Arroyo Quemado (AQUE) and Mohawk (MOHK) kelp forests.

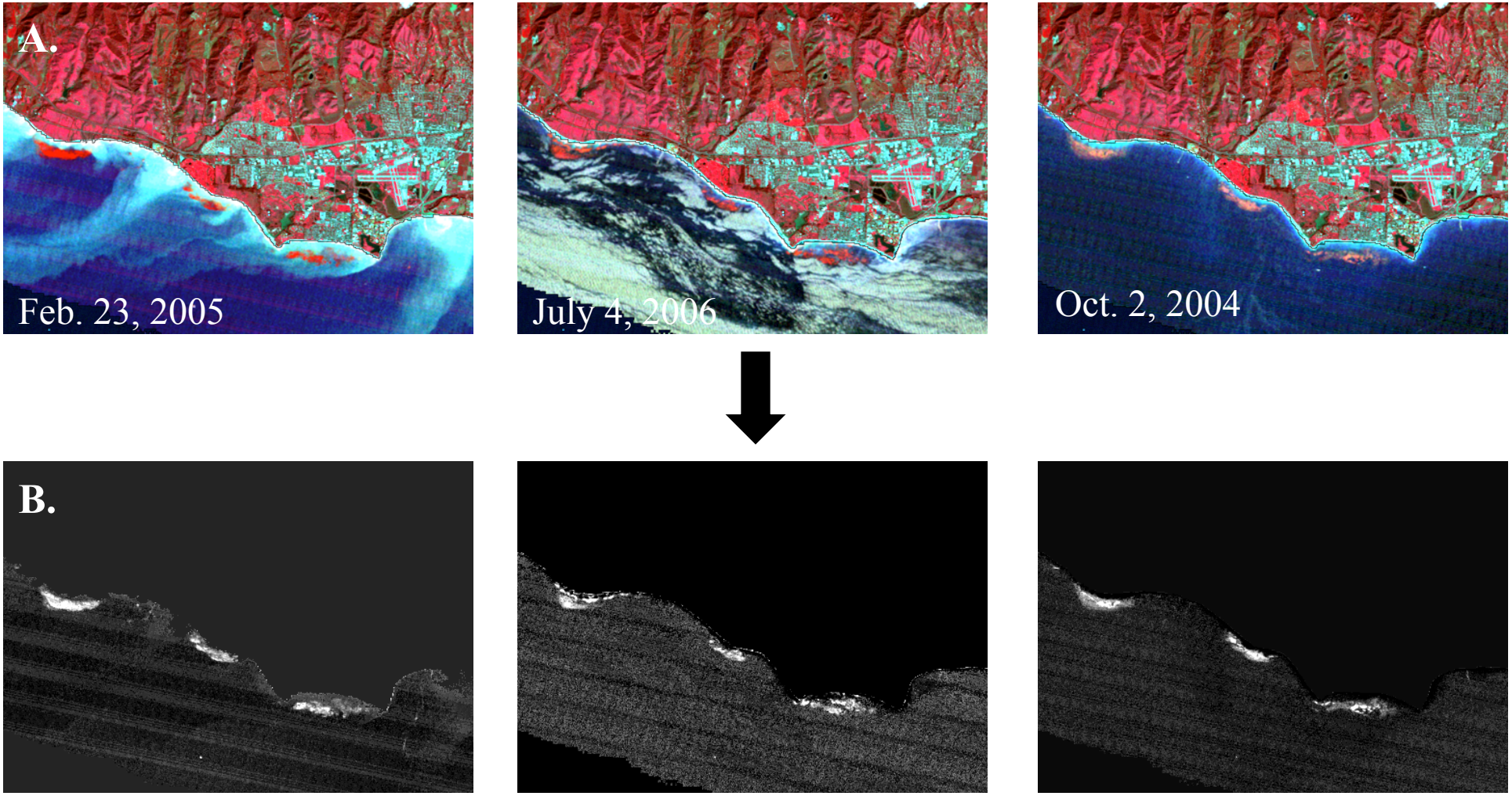

Figure 2. Satellite kelp fraction analysis. (A) LANDSAT false color image of giant kelp beds off Santa Barbara coast. Note variability of water reflectance resulting from sediment runoff in the Feb. 23, 2005 image and glint in the July 4, 2006 image. (B) Kelp fraction images from spectral unmixing process. Brighter pixels correspond to higher kelp fractions. The slight banding apparent in the water is noise that occurs when the detector transitions from bright land targets to dark ocean targets.

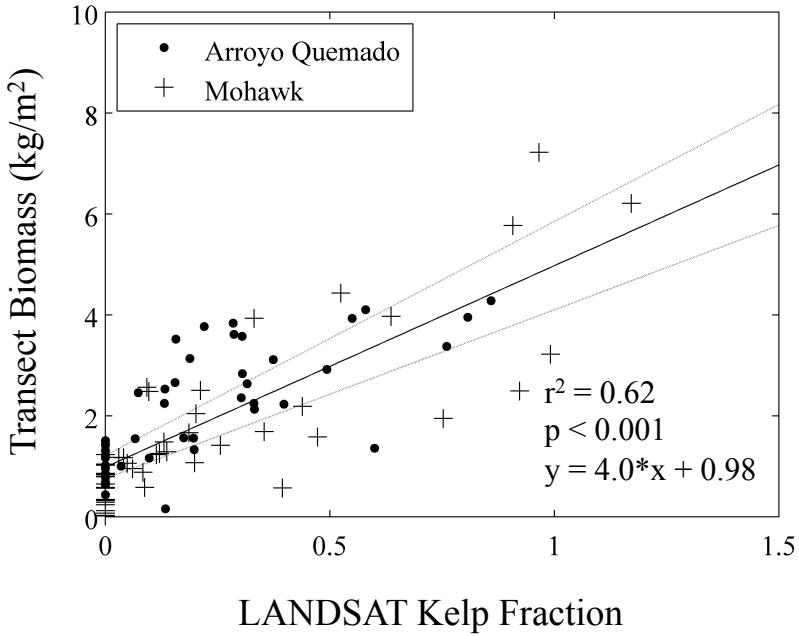

Figure 3. Validation of LANDSAT satellite biomass estimates. Linear regression analysis between LANDSAT kelp fractions and diver measured canopy biomass (kg/m^2) measurements for Arroyo Quemado and Mohawk (n=96). The gray lines represent 95% confidence intervals for the relationship.

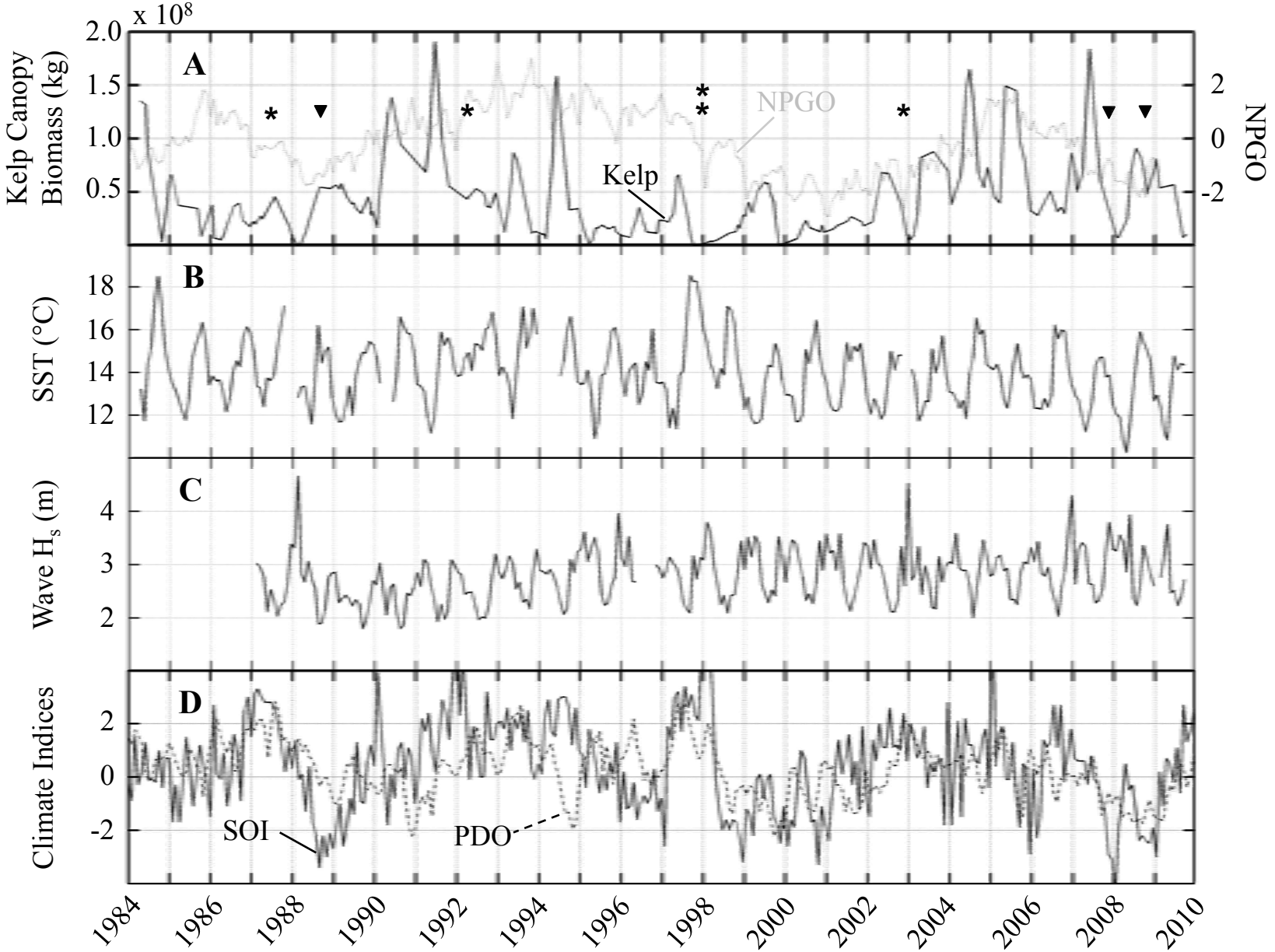

Figure 4. Santa Barbara Channel regional mean time series of (A) giant kelp canopy biomass and NPGO anomalies. Kelp canopy biomass was summed across the entire study area for each image date. 1 month running mean of (B) SST and (C) significant wave height from Pt. Arguello buoy, Harvest platform, and Harvest buoy data. (D) Monthly SOI and PDO anomalies. Asterisks in (A) represent strong El Niño events, with the two asterisks in 1997-1998 identifying the strongest El Niño on record, while triangles represent strong La Niña events (as classified by Smith and Sardeshmukh 2000)

A. Monthly Correlations

	sqrt(kelp)	npgo	pdo	soi	waves
sst	**-0.25**	**0.26**	0.09	**0.19**	**-0.37**
waves	**-0.26**	**-0.17**	-0.01	-0.05	
soi	-0.03	**0.34**	**0.39**		
pdo	**-0.19**	**0.31**			
npgo	0.00				

B. Annual Correlations

	sqrt(kelp)	npgo	pdo	soi	waves
sst	-0.06	**0.60**	**0.53**	**0.62**	-0.40
waves	-0.30	-0.39	0.10	-0.16	
soi	0.19	**0.60**	**0.60**		
pdo	-0.25	**0.54**			
npgo	0.13				

Table 1. Pearson correlation coefficients for regional giant kelp and climactic forcing data calculated on (A) monthly and (B) annual timescales. For the monthly comparisons regional kelp canopy biomass from each image date was correlated to the mean of the physical and climate data from 30 days before the image date. For the annual comparisons the annual mean of kelp was compared to the annual means of SST, SOI, PDO, and NPGO and the annual maximum of wave height. Bold values are significant at the 99% confidence level.

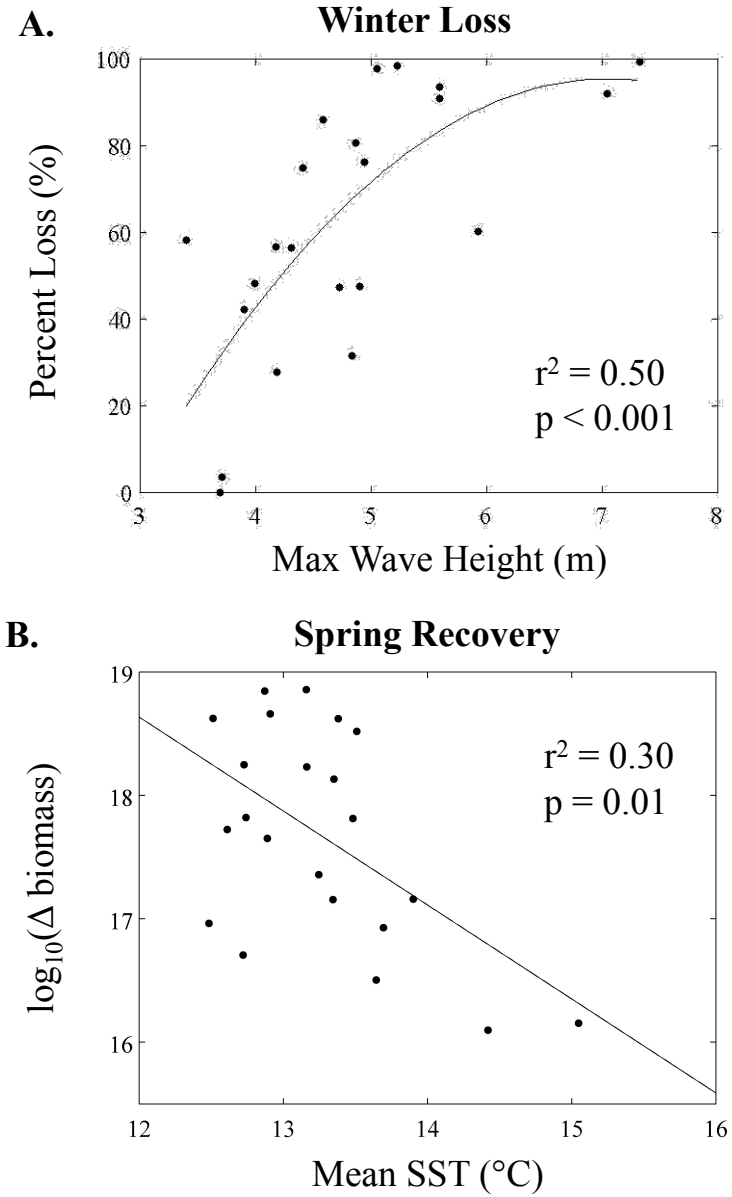

Figure 5. Regression analysis between (A) winter kelp canopy biomass losses and maximum wave height and (B) spring/summer kelp canopy biomass recovery and mean SST. Winter losses were calculated as the change in kelp canopy biomass from the fall (Sept.-Nov.) maximum to the winter/spring (Dec-May) minimum. Recovery represents change in kelp canopy biomass from the winter/spring (Dec-May) minimum to the summer (June-Aug.) maximum. Maximum wave height and mean sst for each year were calculated over the same periods.

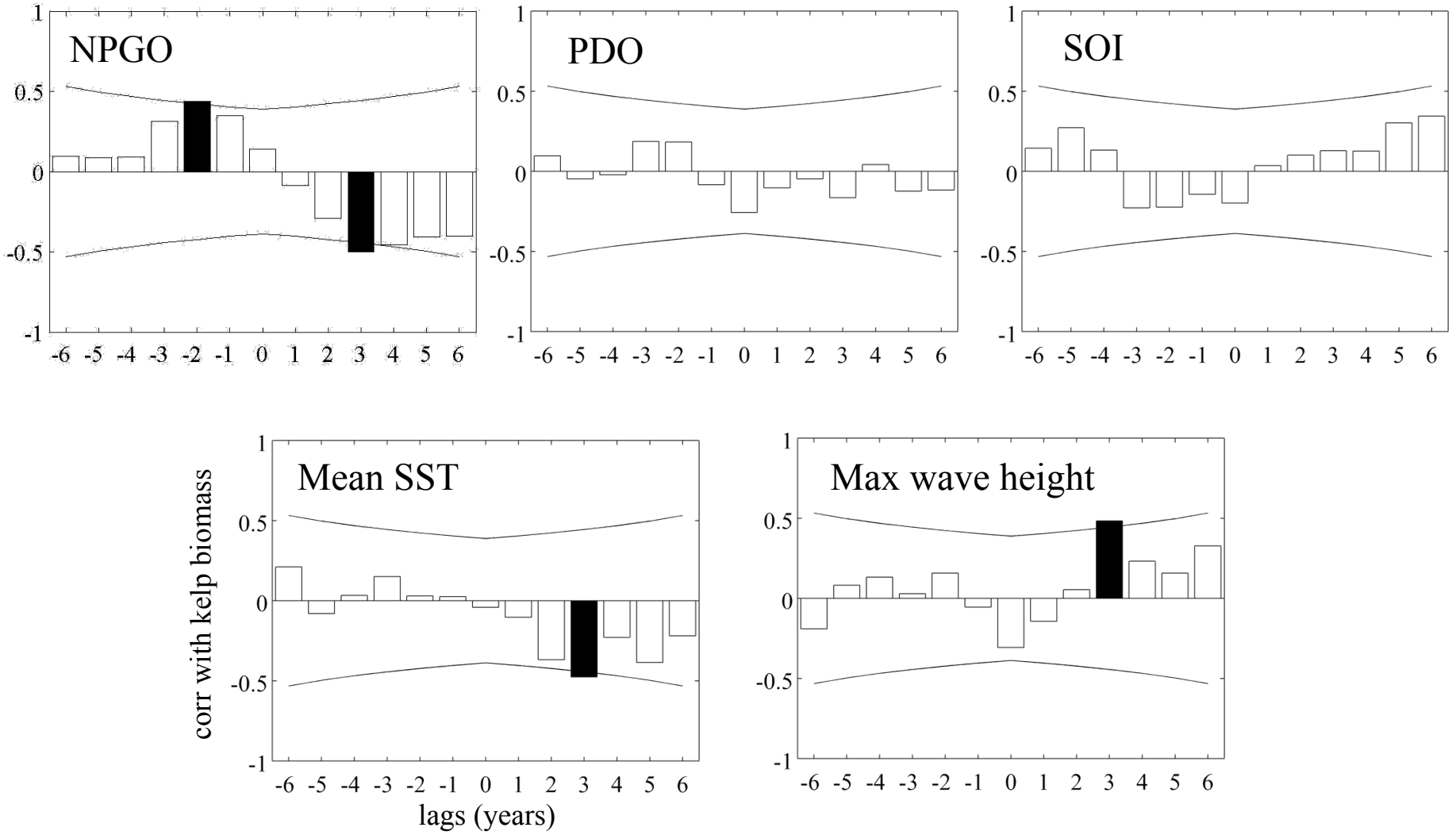

Figure 6. Cross-correlation analysis (at lags of 0-6 years) of climate indices and physical variables on annual mean kelp canopy biomass. Annual mean kelp was compared to mean SST, SOI, PDO, and NPGO and maximum wave height for each year. Bold bars are significant at the 95% level.

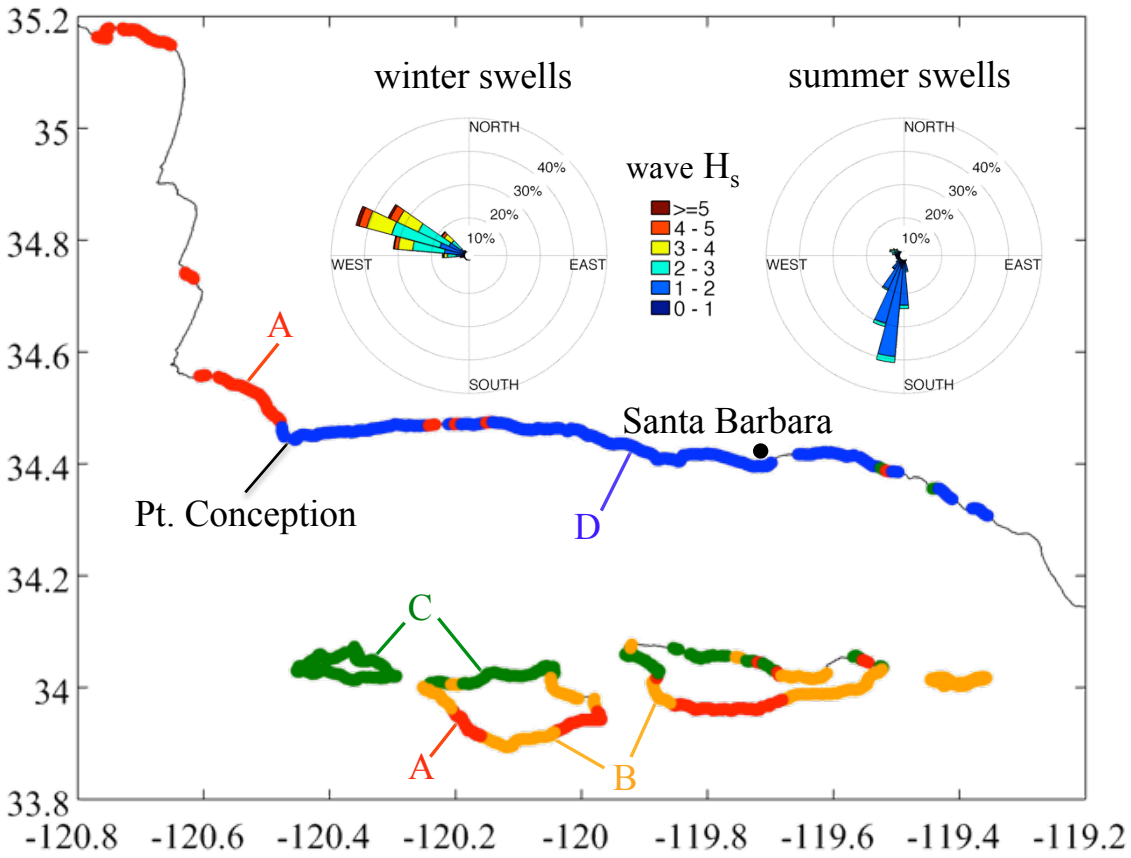

Figure 7. Results from k-means cluster analysis (N=4 clusters) on monthly canopy biomass data binned into 1 km sections of coastline. Subregions are labeled A-D in order of decreasing exposure. Histograms of significant wave height (H_s) and direction for swells with periods larger than 12 seconds are provided for winter (Dec-Feb) and summer (June-August).

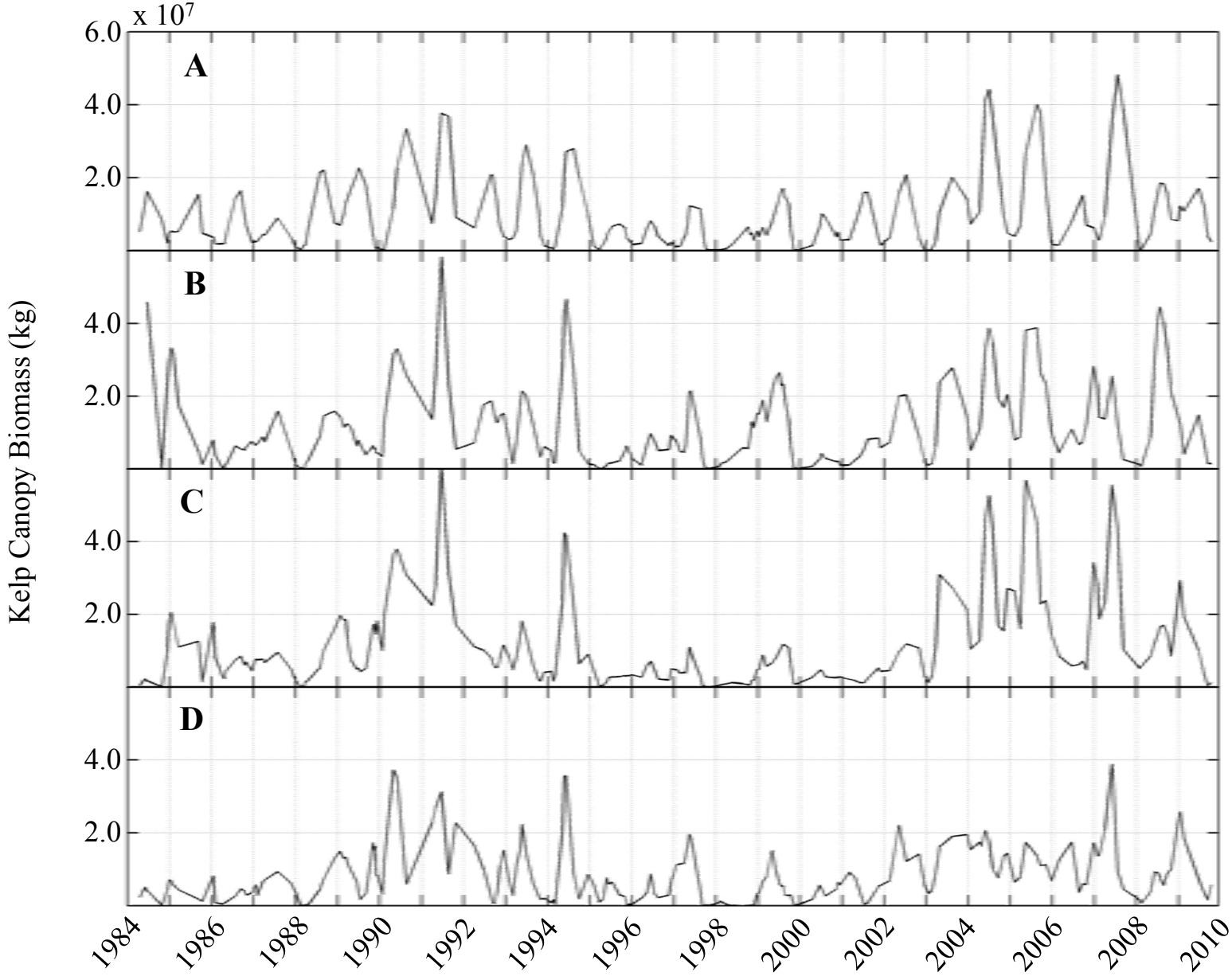

Figure 8. Timeseries of kelp canopy biomass summed across each subregion identified in Figure 7. Subregions are labeled A-D in order of decreasing exposure.

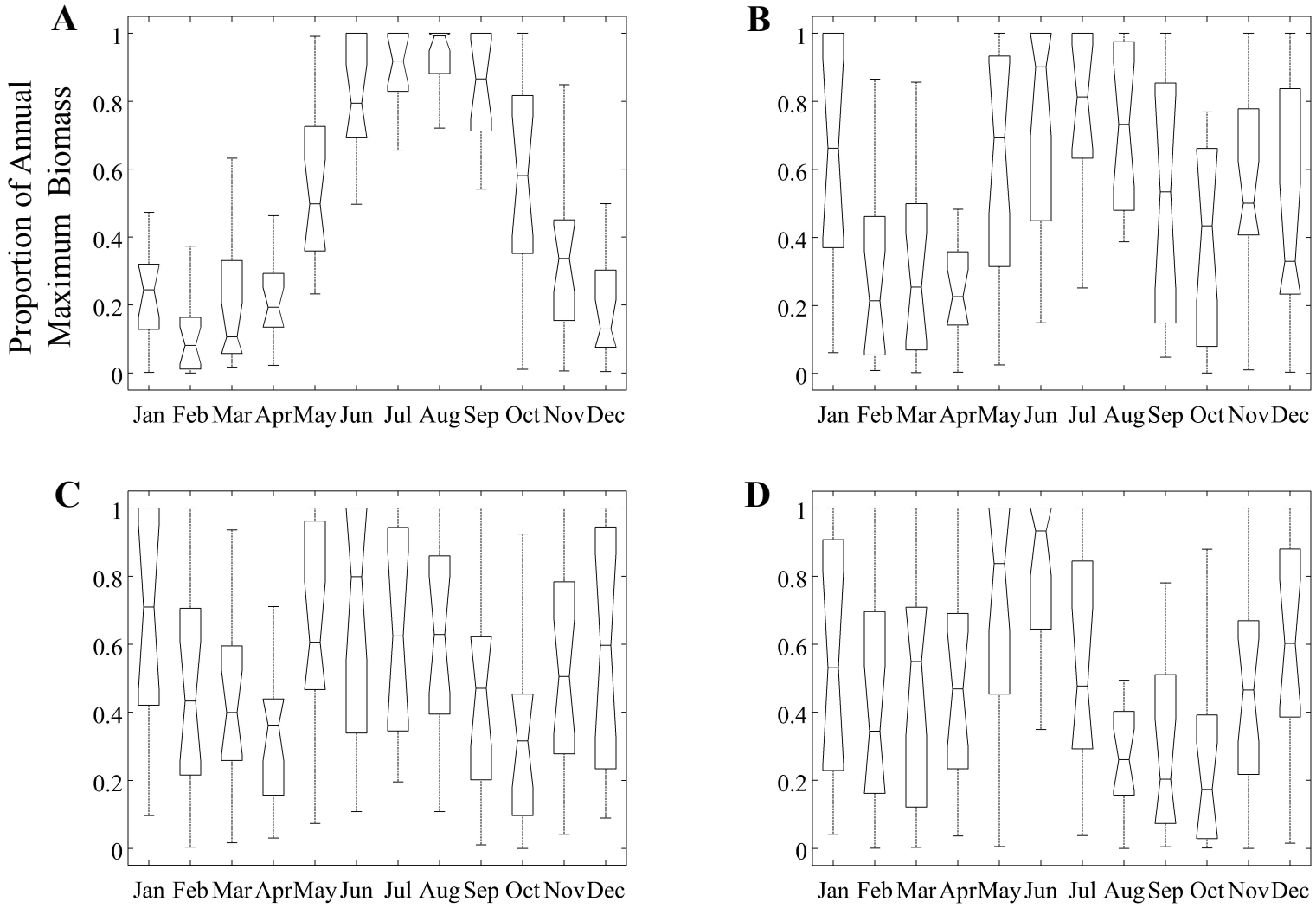

Figure 9. Box and whisker plots of the seasonal cycle in canopy biomass for each subregion. For each year between 1984-2009 the proportion of that year's maximum biomass was calculated for each month. Boxes represent the lower quartile, median, and upper quartile of the proportion of annual maximum biomass and whiskers extend to the lower and upper extremes of the data. Longer boxes represent months with higher variability in their relative canopy biomass levels. Boxes whose notches (not whiskers) do not overlap have significantly different medians at a 95% confidence level.

	A	B	C	D
exposure	11.8	11.6	6.2	4.5
sst corr	-0.04	**-0.17**	**-0.26**	**-0.40**
wave corr	**-0.46**	**-0.24**	-0.15	0.00

Table 2. Mean exposure index and correlation to physical data for each subregion. Subregional kelp from each image date was correlated to the mean of the physical and climate data from 30 days before the image date. Bold values are significant at 99% level.

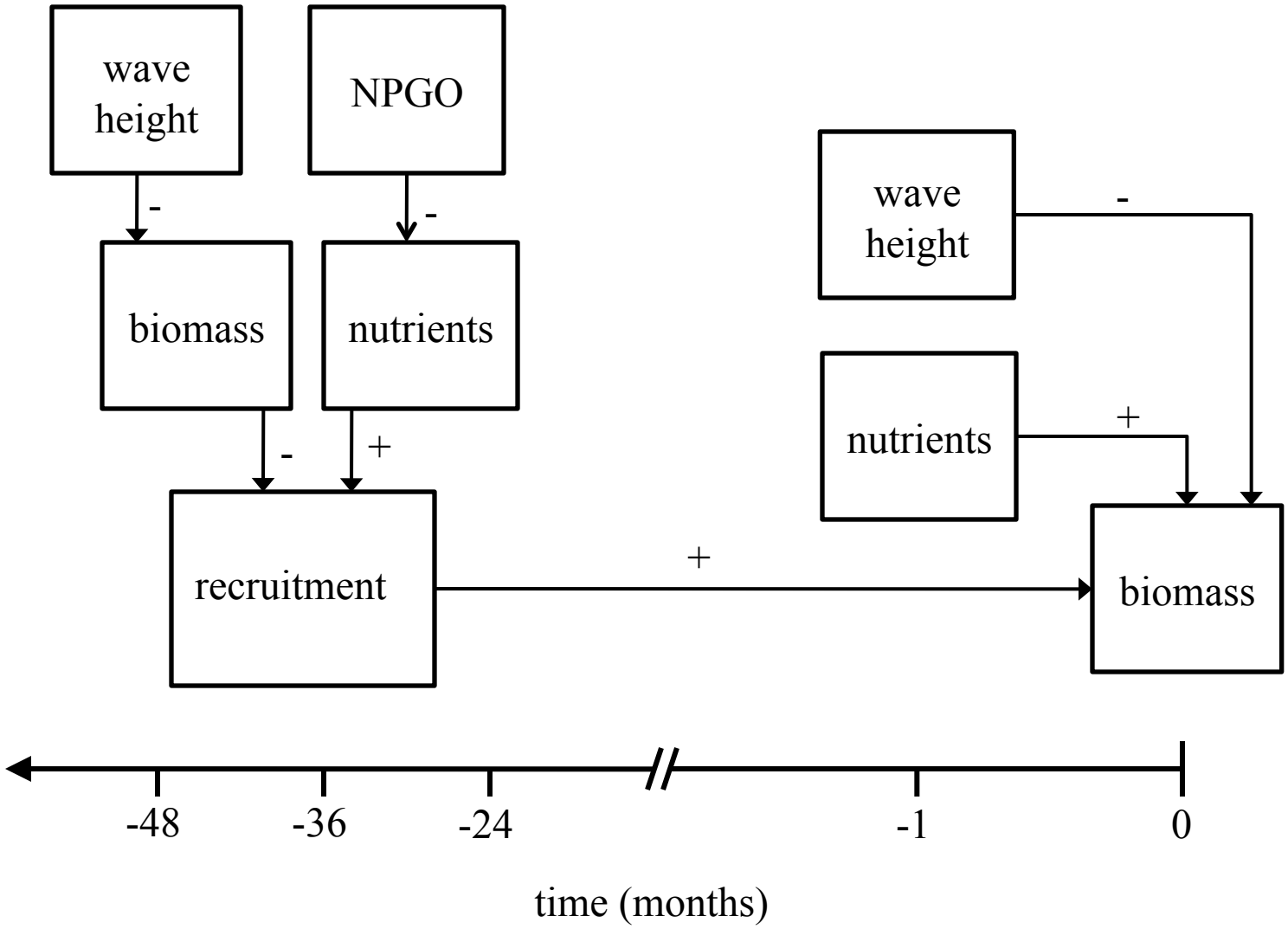

Figure 10. Conceptual model of factors that influence regional giant kelp canopy biomass